NANOSYSTEMS: PHYSICS, CHEMISTRY, MATHEMATICS, 2020, 11 (3), P. 345–354

3D computer models of the T-x-y diagrams, forming the LiF–NaF–CaF_2–LaF_3 T-x-y-z diagram

V. P. Vorob'eva, A. E. Zelenaya, V. I. Lutsyk, M. V. Lamueva

Institute of Physical Materials Science SB RAS, 6, Sakhyanova str., Ulan-Ude, 670047, Russia

vvorobjeva@mail.ru

PACS 81.30.Dz **DOI 10.17586/2220-8054-2020-11-3-345-354**

Giving professor P. P. Fedorov his due as the leading specialist in fluoride systems and using his theoretical investigations on the topology and geometry of phase diagrams of binary and ternary fluoride systems, as well as experimental results, obtained by colleagues under his leadership, the total geometric description of the systems, forming the LiF–NaF–CaF_2–LaF_3 system, which has considerable promise for the development of fourth generation fuels for nuclear reactors, has been received. For this purpose, three-dimensional computer models of all four ternary systems have been constructed and the T-x-y-z diagram of this fluoride system has been predicted.

Keywords: phase diagram, computer model, four-dimensional visualization, lithium fluoride, sodium fluoride, calcium fluoride, lanthanum fluoride.

Received: 3 June 2020

1. Introduction

The compositions obtained from the LiF–NaF–CaF_2–LaF_3 system, as well as many other fluoride systems, are investigated in connection with the development of fourth generation nuclear reactors [1]. In this case, LaF_3 serves as a proxy-compound for PuF_3, since the direct use of PuF_3 would cause enormous experimental difficulties. For the successful design of multicomponent materials, it is very convenient to use spatial (3D – three-dimensional, 4D – four-dimensional) computer models of T-x-y and T-x-y-z diagrams, correspondingly [2, 3]. On the one hand, they generalize the known experimental data and provide opportunities for model adjustment as new knowledge about the system becomes available. On the other hand, the information, accumulated in the 3D model, allows one to understand and to follow the crystallization history of a particular 3-component melt (alloy, ceramic, salts composition).

A huge long-term work on the study of fluoride systems was carried out by professor P. P. Fedorov and colleagues [4–22]. It included a comprehensive experimental study of binary and ternary halide systems, and a theoretical analysis of the topological and geometric features of the obtained phase diagrams. For instance, saddle points on the liquidus surfaces, associated with the congruent nature of melting, were experimentally discovered [20, 21] in the systems BaF_2–SrF_2–LaF_3 [10], PbF_2–CdF_2–RF_3 (R=Er, Lu) [18], CaF_2–SrF_2–RF_3 (R=La, Nd, Yb) [19]. It was shown that the conjugate surfaces of the liquidus and solidus can have a singular point of the saddle type [22], and the saddle point on the surface of the diagram appears if the liquidus of two boundary binary systems has a minimum and the third one has a maximum or vice versa.

The surfaces of the phase diagrams formed by the fluorides of lithium, sodium, calcium, and lanthanum are not so complicated; they haven't the saddle or extrema points. But the geometric structure of these diagrams becomes more complicated by the formation of the binary $NaLaF_4$ compound and polymorphism of CaF_2 [23]. 3D models are constructed on the basis of data on binary systems, projections of liquidus surfaces with isothermal lines, drawn on them.

2. Binary and ternary systems, forming the LiF–NaF–CaF_2–LaF_3 T-x-y-z diagram

Before designing a computer 3D (and 4D too) model, it is necessary to discuss the boundary systems [23], as well as to make a formal indication of the quaternary system under consideration, that is, to indicate the LiF–NaF–CaF_2-LaF_3 system as A-B-C-D, and to give the necessary indication of all phase transformations. For example, two polymorphic modifications of CaF_2 are involved in the formation of the LiF–NaF–CaF_2–LaF_3 (A-B-C-D) diagram and they received the appropriate indicators: C and C1.

The systems LiF–NaF (A-B) and LiF–LaF_3 (A-D) are eutectic ones, LiF–CaF_2 (A-C) and NaF–CaF_2 (B-C) are also of eutectic type, but they include a polymorphic transition in the form of the metatectic reaction (C $\to$ C1 + L), due to the allotropy of calcium fluoride (CaF_2).

The incongruently melting $NaLaF_4$ (R) compound is formed in the NaF–LaF_3 (B-D) system and two reactions – peritectic p_{DR}: L + D $\to$ R and eutectic e_{BR}: L $\to$ B + R – take a place.

The eutectic CaF_2–LaF_3 (C-D) system is characterized by the eutectoid reaction C $\rightarrow$ C1 + D because of the polymorphism of calcium fluoride.

The ternary eutectic system LiF–NaF–CaF_2 (A-B-C) with a single invariant reaction E_1: L $\rightarrow$ A + B + C1 is complicated by the univariant polymorphic C $\rightarrow$ C1 + L transition between two CaF_2 modifications (Fig. 1a).

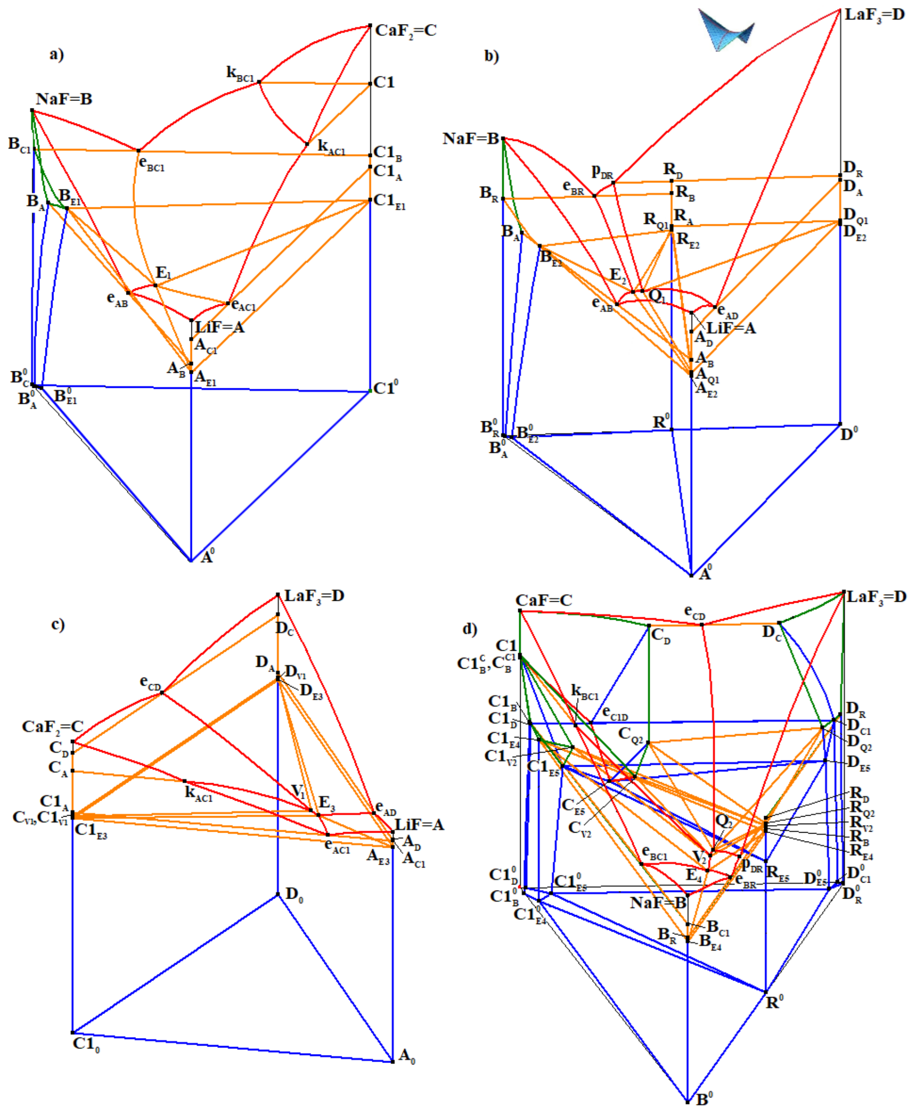

FIG. 1. 3D computer models of T-x-y diagrams LiF–NaF–CaF_2 (A-B-C) (a), LiF–NaF–LaF_3 (A-B-D) (b), LiF–CaF_2–LaF_3 (A-C-D) (c) – simplified model, NaF–CaF_2–LaF_3 (B-C-D) (d)

The system LiF–NaF–LaF_3 (A-B-D) with the $NaLaF_4$ (R) binary incongruently melting compound is characterized by quasi-peritectic Q_1: L + D $\rightarrow$ A + R and eutectic E_2: L $\rightarrow$ A + B + R invariant reactions (Fig. 1b).

There are two invariant transformations in the LiF–CaF_2–LaF_3 (A-C-D) system (Fig. 1c). One of them is the eutectic reaction E_3: L $\rightarrow$ A + D + C1. The second one in [23] is called a quasi-peritectic reaction and is written as L + C $\rightarrow$ C1 + D. However, it is not. Since the C $\rightarrow$ C1 + L polymorphic transition in the A-C binary system is associated with this reaction, the V_1: C $\rightarrow$ C1 + D + L polymorphic transition also takes a place in the ternary system, formed by it, with the passive role of the L and LaF_3 (D). More details on ternary systems with allotropy of components, including a similar case, are described in the paper [24].

A similar polymorphic transition V_2: C $\rightarrow$ C1 + R + L takes a place in the NaF–CaF_2–LaF_3 (B-C-D) system. This reaction is intermediate between two other invariant reactions, quasi-peritectic Q_2: L + D $\rightarrow$ C + R and eutectic E_4: L $\rightarrow$ B + R + C1 (Fig. 1d). The logic of phase reactions leads to the fact that it should expect another invariant reaction – the eutectoid one E_5: C $\rightarrow$ C1 + D + R. The scheme of uni- and invariant states of this system (Table 1), as well as three other geometrically simpler systems (Fig. 1a–c), gives a possibility to describe all surfaces (Table 2) and all phase regions (Table 3) of the NaF–CaF$_2$–LaF$_3$ (B-C-D) T-x-y diagram.

TABLE 1. The scheme of uni- and invariant states of the NaF–CaF$_2$–LaF$_3$ (B-C-D) T-x-y diagram with the NaLaF$_4$ (R) incongruently melting compound and CaF$_2$ allotropy (Fig. 1d), D>C>e_{CD} >k_{BC1} >B>e_{BC1} >p_{DR} >Q$_2$ >V$_2$ >e_{BR} >e_{C1D} >E$_4$ >E$_5$

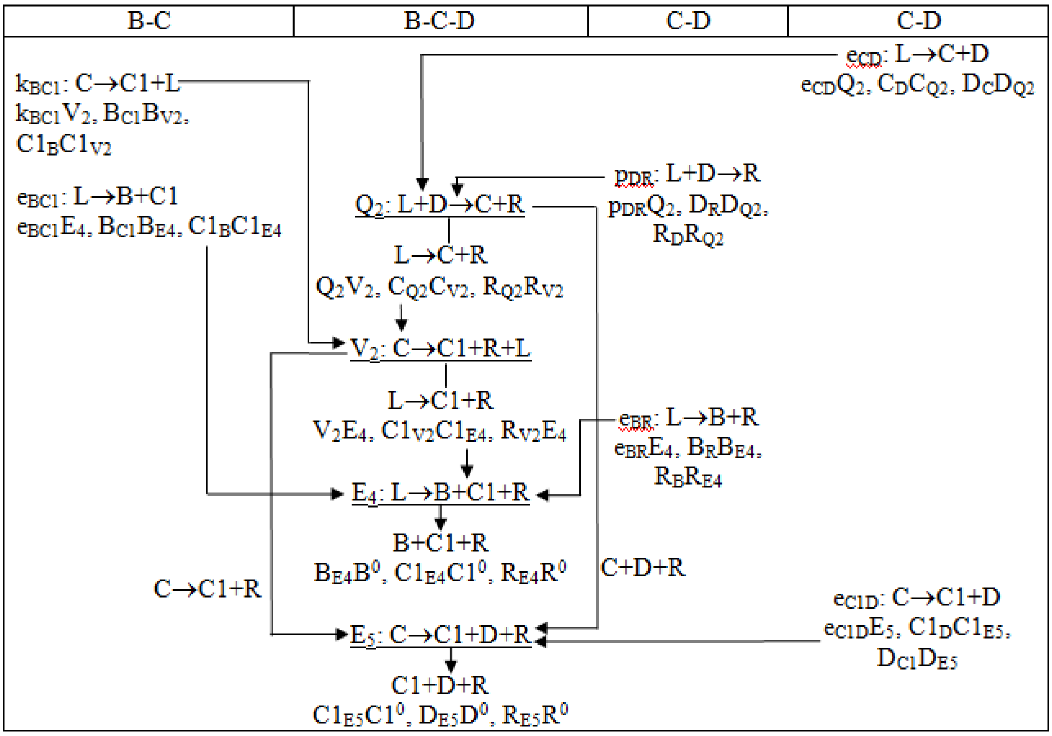

Three-dimensional (3D) computer models allow to get any isothermal section (Fig. 2a) or isopleth (Fig. 2b).

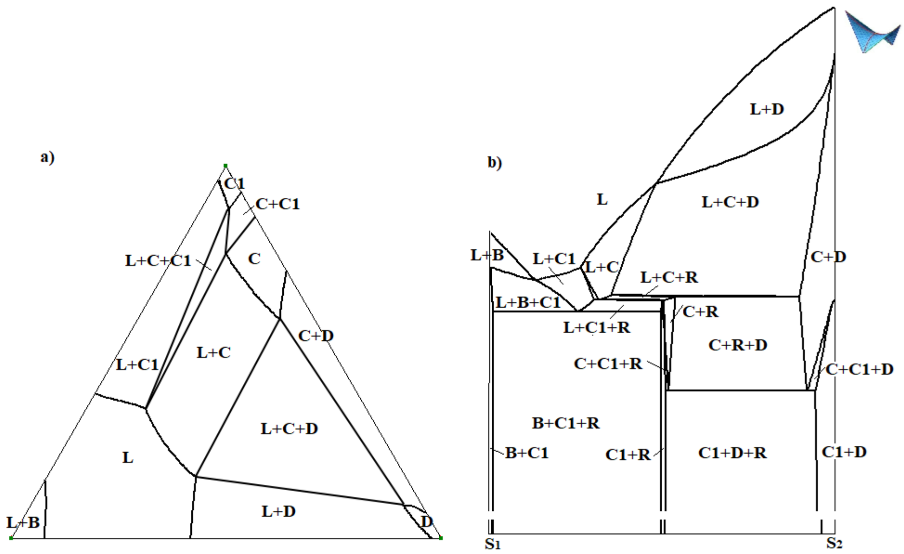

FIG. 2. Isothermal section at 1200 K (a) and isopleth S$_1$(0.8, 0.2, 0)–S$_2$(0, 0.2, 0.8) (b) of the NaF–CaF$_2$–LaF$_3$ (B–C–D) T-x-y diagram 3D model

To visualize the results of calculations of mass balances of coexisting phases, mass balance diagrams (DMB) are used [25]. Such DMB, called vertical (VDMB) one (Fig. 3a), is able to show not only the phase ratios for a given mass

TABLE 2. Surfaces of the NaF–CaF_2–LaF_3 (B-C-D) T-x-y diagram with the $NaLaF_4$ (R) incongruently melting compound (Fig. 1d)

No	Designation	Points of contour	No	Designation	Points of contour
liquidus – solidus					
1	q_B	$Be_{BC1}E_4e_{BR}$	6	s_B	$BB_{C1}B_{E4}B_R$
2	q_C	$Ck_{BC1}V_2Q_2e_{CD}$	7	s_C	$CC^{C1}{}_BC_{V2}C_{Q2}C_D$
3	q_{C1}	$k_{BC1}V_2E_4e_{BC1}$	8	s_{C1}	$C1^C{}_BC1_{V2}C1_{E4}C1_B$
4	q_D	$Dp_{DR}Q_2e_{CD}$	9	s_D	$DD_RD_{Q2}D_C$
5	q_R	$p_{DR}e_{BR}E_4V_2Q_2$	10	s_R	$R_DR_BR_{E4}R_{V2}R_{Q2}$
transus					
11	t^q	$C1C^{C1}{}_Be_{C1D}C_{E5}C_{V2}$	12	t^s	$C1C1^C{}_BC1_DC1_{E5}C1_{V2}$
solvus					
13	v_{BC1}	$B_{C1}B_{E4}B^0{}_{E4}B^0{}_{C1}$	20	v_{C1B}	$C1_BC1_{E4}C1^0{}_{E4}C1^0{}_B$
14	v_{BR}	$B_RB_{E4}B^0{}_{E4}B^0{}_R$	21	v_{RB}	$R_BR_{E4}R^0{}_{E4}R^0{}_B$
15	v_{CD}	$C_De_{C1D}C_{E5}C_{Q2}$	22	v_{DC}	$D_CD_{C1}D_{E5}D_{Q2}$
16	v_{CR}	$C_{Q2}C_{V2}C_{E5}$	23	v_{RC}	$R_{Q2}R_{V2}R_{E5}$
17	v_{C1R}	$C1_{V2}C1_{E4}C1^0{}_{E4}C1^0{}_{E5}C1_{E5}$	24	v_{RC1}	$R_{V2}R_{E4}R^0{}_{E4}R^0{}_{E5}R_{E5}$
18	v_{DR}	$D_RD_{Q2}D_{E5}D^0{}_{E5}D^0{}_R$	25	v_{RD}	$R_DR_{Q2}R_{E5}R^0{}_{E5}R^0{}_D$
19	v_{C1D}	$C1_DC1_{E5}C1^0{}_{E5}C1^0{}_D$	26	v_{D1}	$D_{C1}D_{E5}D^0{}_{E5}D^0{}_{C1}$
ruled surfaces					
27	$q^r{}_{BC1}$	$e_{BC1}E_4$-$B_{C1}B_{E4}$	45	$q^r{}_{BR}$	$e_{BR}E_4$-B_RB_{E4}
28	$q^r{}_{C1B}$	$e_{BC1}E_4$-$C1_BC1_{E4}$	46	$q^r{}_{RB}$	$e_{BR}E_4$-R_BR_{E4}
29	$s^r{}_{BC1}$	$B_{C1}B_{E4}$-$C1_BC1_{E4}$	47	$s^r{}_{BR}$	B_RB_{E4}-R_BR_{E4}
30	$q^r{}_{CD}$	$e_{CD}Q_2$-C_DC_{Q2}	48	$q^r{}_{CR}$	Q_2V_2-$C_{Q2}C_{V2}$
31	$q^r{}_{DC}$	$e_{CD}Q_2$-D_CD_{Q2}	49	$q^r{}_{RC}$	Q_2V_2-$R_{Q2}R_{V2}$
32	$s^r{}_{CD}$	C_DC_{Q2}-D_CD_{Q2}	50	$s^r{}_{CR}$	$C_{Q2}C_{V2}$-$R_{Q2}R_{V2}$
33	$q^r{}_{C1R}$	V_2E_4-$C1_{V2}C1_{E4}$	51	$q^r{}_{DR}$	$p_{DR}Q_2$-D_RD_{Q2}
34	$q^r{}_{RC1}$	V_2E_4-$R_{V2}R_{E4}$	52	$q^r{}_{RD}$	$p_{DR}Q_2$-R_DR_{Q2}
35	$s^r{}_{C1R}$	$C1_{V2}C1_{E4}$-$R_{V2}R_{E4}$	53	$s^r{}_{DR}$	D_RD_{Q2}-R_DR_{Q2}
36	$q^r{}_{CC1}$	$k_{BC1}V_2$-$C^{C1}{}_BC_{V2}$	54	$q^{rC}{}_{C1D}$	$e_{C1D}C_{E5}$-$C1_DC1_{E5}$
37	$q^r{}_{C1C}$	$k_{BC1}V_2$-$C1^C{}_BC1_{V2}$	55	$q^{rC}{}_{DC1}$	$e_{C1D}C_{E5}$-$D_{C1}D_{E5}$
38	$s^r{}_{CC1}$	$C^{C1}{}_BC_{V2}$-$C1^C{}_BC1_{V2}$	56	$s^{rC}{}_{C1D}$	$C1_DC1_{E5}$-$D_{C1}D_{E5}$
39	$q^{rC}{}_{C1R}$	$C_{V2}C_{E5}$-$C1_{V2}C1_{E5}$	57	$v^r{}_{CD(Q2)}$	$C_{Q2}C_{E5}$-$D_{Q2}D_{E5}$
40	$q^{rC}{}_{RC1}$	$C_{V2}C_{E5}$-$R_{V2}R_{E5}$	58	$v^r{}_{CR(Q2)}$	$C_{Q2}C_{E5}$-$R_{Q2}R_{E5}$
41	$s^{rC}{}_{C1R}$	$C1_{V2}C1_{E5}$-$R_{V2}R_{E5}$	59	$v^r{}_{DR(Q2)}$	$D_{Q2}D_{E5}$-$R_{Q2}R_{E5}$
42	$v^r{}_{BC1(E4)}$	$B_{E4}B^0{}_{E4}$-$C1_{E4}C1^0{}_{E4}$	60	$v^r{}_{C1D(E5)}$	$C_{E5}C^0{}_{E5}$-$D_{E5}D^0{}_{E5}$
43	$v^r{}_{BR(E4)}$	$B_{E4}B^0{}_{E4}$-$R_{E4}R^0{}_{E4}$	61	$v^r{}_{C1R(E5)}$	$C1_{E5}C1^0{}_{E5}$-$R_{E5}R^0{}_{E5}$
44	$v^r{}_{C1R(E4)}$	$C1_{E4}C1^0{}_{E4}$-$R_{E4}R^0{}_{E4}$	62	$v^r{}_{DR(E5)}$	$D_{E5}D^0{}_{E5}$-$R_{E5}R^0{}_{E5}$
horizontal planes					
63	$h^{Q2}{}_{CDR}$	$C_{Q2}D_{Q2}R_{Q2}$	71	$h^{V2}{}_{CC1R}$	$C_{V2}C1_{V2}R_{V2}$
64	h_{CDQ2}	$C_{Q2}D_{Q2}Q2$	72	h_{CC1V2}	$C_{V2}C1_{V2}V2$
65	h_{CRQ2}	$C_{Q2}R_{Q2}Q2$	73	h_{CRV2}	$C_{V2}R_{V2}V2$
66	h_{DRQ2}	$D_{Q2}R_{Q2}Q2$	74	h_{C1RV2}	$C1_{V2}R_{V2}V2$
67	$h^{E4}{}_{BC1R}$	$B_{E4}C1_{E4}R_{E4}$	75	$h^{E5}{}_{CC1D}$	$C_{E5}C1_{E5}D_{E5}$
68	h_{BC1E4}	$B_{E4}C1_{E4}E4$	76	$h^{E5}{}_{CC1R}$	$C_{E5}C1_{E5}R_{E5}$
69	h_{BRE4}	$C_{E4}R_{E4}E4$	77	$h^{E5}{}_{CDR}$	$C_{E5}D_{E5}R_{E5}$
70	h_{C1RE4}	$C1_{E4}R_{E4}E4$	78	$h^{E5}{}_{C1DR}$	$C1_{E5}D_{E5}R_{E5}$

TABLE 3. Phase regions of the NaF–CaF_2–LaF_3 (B-C-D) T-x-y diagram with the $NaLaF_4$ (R) incongruently melting compound (Fig. 1d)

No	Phase region	Border hypersurfaces	Adjacent phase regions
1	L+B	q_B, s_B, q^r_{BC1}, q^r_{BR}	L, B, L+B+C1, L+B+R
2	L+C	q_C, s_C, q^r_{CD}, q^r_{CR}, q^r_{CC1}	L, C, L+C+D, L+C+R, L+C+C1
3	L+C1	q_{C1}, s_{C1}, q^r_{C1B}, q^r_{C1C}, q^r_{C1R}	L, C1, L+B+C1, L+C+C1, L+C1+R
4	L+D	q_D, s_D, q^r_{DC}, q^r_{DR}	L, D, L+C+D, L+D+R
5	L+R	q_R, s_R, q^r_{RB}, q^r_{RC}, q^r_{RC1}, q^r_{RD}	L, R, L+B+R, L+C+R, L+C1+R, L+D+R
6	L+B+C1	q^r_{BC1}, q^r_{C1B}, s^r_{BC1}, h_{BC1E4}	L+B, L+C1, B+C1, L+B+C1+R
7	L+B+R	q^r_{BR}, q^r_{RB}, s^r_{BR}, h_{BRE4}	L+B, L+R, B+R, L+B+C1+R
8	L+C+D	q^r_{CD}, q^r_{DC}, s^r_{CD}, h_{CDQ2}	L+C, L+D, C+D, L+C+D+R
9	L+C+R	q^r_{CR}, q^r_{RC}, s^r_{CR}, h_{CRQ2}, h_{CRV2}	L+C, L+R, C+R, L+C+D+R, L+C+C1+R
10	L+C1+R	q^r_{C1R}, q^r_{RC1}, s^r_{C1R}, h_{C1RV2}, h_{C1RE4}	L+C1, L+R, C1+R, L+C+C1+R, L+B+C1+R
11	L+D+R	q^r_{DR}, q^r_{RD}, s^r_{DR}, h_{DRQ2}	L+D, L+R, D+R, L+C+D+R
12	L+C+C1	q^r_{CC1}, q^r_{C1C}, s^r_{CC1}, h_{CC1V2}	L+C, L+C1, C+C1, L+C+C1+R
13	B	s_B, v_{BC1}, v_{BR}	L+B, B+C1, B+R
14	C	s_C, v_{CD}, v_{CR}, t^q	L+C, C+D, C+R, C+C1
15	C1	t^s, s_{C1}, v_{C1B}, v_{C1D}, v_{C1R}	C+C1, L+C1, B+C1, C1+D, C1+R
16	D	s_D, v_{DC}, v_{DR}, v_{DC1}	L+D, C+D, D+R, C1+D
17	R	s_R, v_{RB}, v_{RC}, v_{RC1}, v_{RD}	L+R, B+R, C+R, C1+R, D+R
18	B+C1	v_{BC1}, v_{C1B}, s^r_{BC1}, $v^r_{BC1(E4)}$	B, C1, L+B+C1, B+C1+R
19	B+R	v_{BR}, v_{RB}, s^r_{BR}, $v^r_{BR(E4)}$	B, R, L+B+R, B+C1+R
20	C+R	v_{CR}, v_{RC}, s^r_{CR}, $v^r_{CR(Q2)}$, s^{rC}_{C1R}	C, R, L+C+R, C+D+R, C+C1+R
21	C+D	v_{CD}, v_{DC}, s^r_{CD}, $v^r_{CD(Q2)}$, s^{rC}_{C1D}	C, D, L+C+D, C+D+R, C+C1+D
22	C1+R	v_{C1R}, v_{RC1}, s^r_{C1R}, $v^r_{C1R(E4)}$, q^{rC}_{C1R}, $v^r_{C1R(E5)}$	C1, R, L+C1+R, B+C1+R, C+C1+R, C1+D+R
23	C1+D	v_{C1D}, v_{DC1}, q^{rC}_{C1D}, $v^r_{C1D(E5)}$	C1, D, C+C1+D, C1+D+R
24	D+R	v_{DR}, v_{RD}, s^r_{DR}, $v^r_{DR(Q2)}$, $v^r_{DR(E5)}$	D, R, L+D+R, C+D+R, C1+D+R
25	B+C1+R	$v^r_{BC1(E4)}$, $v^r_{BR(E4)}$, $v^r_{C1R(E4)}$, h^{E4}_{BC1R}	B+C1, B+R, C1+R, L+B+C1+R
26	C+C1+D	q^{rC}_{C1D}, q^{rC}_{DC1}, s^{rC}_{C1D}, h^{E5}_{CC1D}	C+C1, C+D, C1+D, C+C1+D+R
27	C+C1+R	q^{rC}_{C1R}, q^{rC}_{RC1}, s^{rC}_{C1R}, h^{V2}_{CC1R}, h^{E5}_{CC1R}	C+C1, C+R, C1+R, L+C+C1+R, C+C1+D+R
28	C+D+R	$v^r_{CD(Q2)}$, $v^r_{CR(Q2)}$, $v^r_{DR(Q2)}$, h^{Q2}_{CDR}, h^{E5}_{CDR}	C+D, C+R, D+R, L+C+D+R, C+C1+D+R
29	C1+D+R	v^r_{C1D}, v^r_{C1R}, v^r_{DR}, h^{E5}_{C1DR}	C1+D, C1+R, D+R, C+C1+D+R

center G at a fixed temperature, but also to observe the crystallization of liquid over the entire temperature range. The crystallization pathways (Fig. 3b) were considered earlier in ternary oxide and salt systems [26].

Projection of all surfaces of the T-x-y diagram onto the temperature-free x-y triangle divides it into a concentration fields. Each field differs from the others in the sequence of phase reactions and, accordingly, in the unique crystallization history (Fig. 3a). E.g., mass center G (0.368, 0.416, 0.216) (Fig. 3b), cuts 4 phase regions: L + C, L + C + C1, L + C1 + R, B + C1 + R. It's understandable from the VDMB (Fig. 3a), that a vertical line in point G cuts liquidus surface q_C and appears in the 2-phase region L + C, where a reaction of primary crystallization L $\to$ C^1 proceeds. Then it cuts the ruled surface q^r_{CC1}, passing the 3-phase region L + C + C1, with the peritectic reaction L + C $\to$ $C1^{p(C)}$, with a decrease in phases C and L share, simultaneously with the C1 phase share increasing. There is the polymorphic transition V_2: C $\to$ $C1^{V2}$ + R^{V2} + L^{V2} at 1016 K. As a result of this reaction, the crystals C is fully expended. After the postperitectic secondary reaction L + C1 $\to$ $R^{pp(C1)}$ occurs in the three-phase region L + R + C1 and the resulting by the invariant eutectic reaction E_4: L $\to$ B^{E4} + R^{E4} + $C1^{E4}$ on the horizontal plane. There is the

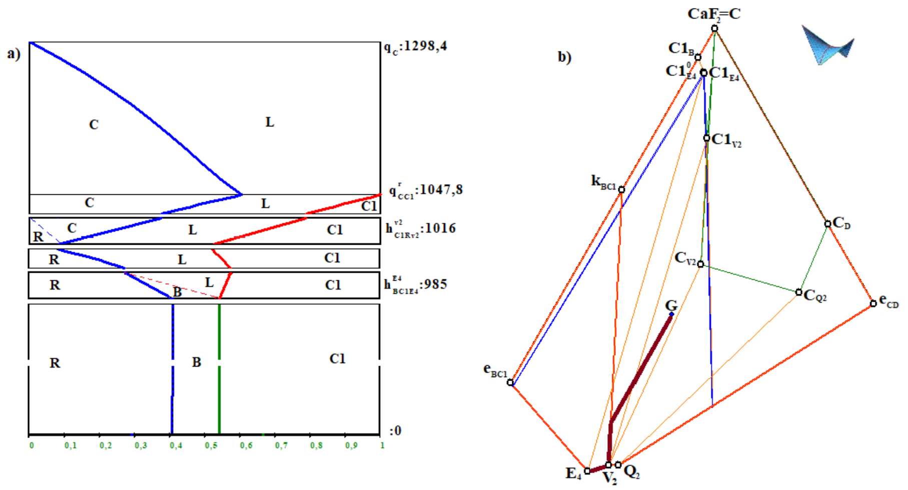

FIG. 3. Vertical mass balance diagram for the mass center G (0.368, 0.416, 0.216) (a), fragment of the x-y projection of the NaF–CaF$_2$–LaF$_3$ (B-C-D) T-x-y diagram with the crystallization path for G

sub-solidus 3-phase region B + C1 + R below this plane. So, the mass center G can be characterized by the next set of the microstructural elements: C1$^{p(C)}$, C1^{V2}, R^{V2}, R$^{pp(C1)}$, B^{E4}, R^{E4}, C1^{E4}.

Presented at the VDMB crystallization stages are confirmed by the calculation of crystallization paths for the given composition (Fig. 3b).

Another option for DMB is the horizontal mass balance diagram (HDMB) (Fig. 4a). It is added to the isopleth and shows the ratios of coexisting phases for all compositions in this section at a fixed temperature (Fig. 4b). The electrical conductivity curve during melt crystallization (Fig. 4c) is performed too.

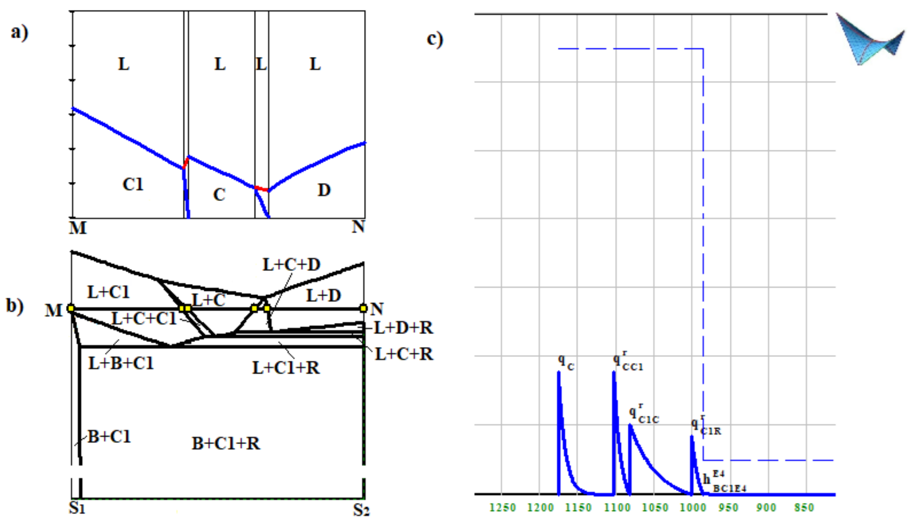

FIG. 4. Horizontal mass balance diagram at $T = 1100$ K (a) for the S$_1$(0.5, 0.5, 0)–S$_2$(0.5, 0, 0.5) isopleth (b), imitation of the DTA-spectra and the electrical conductivity leap for G(0.368,0.416,0.216) (c) in the NaF–CaF$_2$–LaF$_3$ (B-C-D) T-x-y diagram

Thus, a 3D computer model provides an excellent opportunity to obtain a complete and comprehensive view of the T-x-y diagram, either its geometric structure or the options for its melts crystallization. In addition, 3D models are very useful as for their structures understanding and for the 4D model designing of the four-component system T-x-y-z diagram, formed by them.

3. Prediction and prototype design of the LiF–NaF–CaF$_2$–LaF$_3$ T-x-y-z diagram 4D computer model

Construction of the 3D computer model of the T-x-y diagram begins with the 3D scheme of uni- and invariant states [24,25]. This is a 3D variant of well-known scheme of phase reactions (planar Sheil scheme [27]), supplemented by the concentrations of phases, which participate in three-phase transformations. This very important addition opens wide possibilities for describing all surfaces and phase regions of the T-x-y diagram (as it is shown by the point's designation in Tables 1–3). The same approach is applied to design the 4D computer model of the T-x-y-z diagram. As for the LiF–NaF–CaF$_2$–LaF$_3$ system, the logic of the uni- and invariant state schemes of the forming ternary systems leads to the only possible scheme of the phase reactions of the quaternary system (Table 4). If it is supplemented and similarly expanded to a scheme of di-, uni-, and invariant states, then a full formal description of all hypersurfaces and phase regions can be obtained.

TABLE 4. The phase reactions scheme of the LiF–NaF–CaF$_2$–LaF$_3$ (A-B-C-D) T-x-y-z diagram with the incongruently melting compound NaLaF$_4$ (R) and CaF$_2$ (C, C1) allotropy (Fig. 5), D>C>e_{CD} >k_{AC1} = k_{BC1} >B>A>e_{BC1} >p_{DR} >e_{AD} >e_{AC1} >Q$_2$ >V$_2$ >e_{BR} >V$_1$ >e_{C1D} > E$_4$ >E$_3$ >e_{AB} >E$_1$ >Q$_1$ >E$_2$ >E$_5$ > ν > π > ε

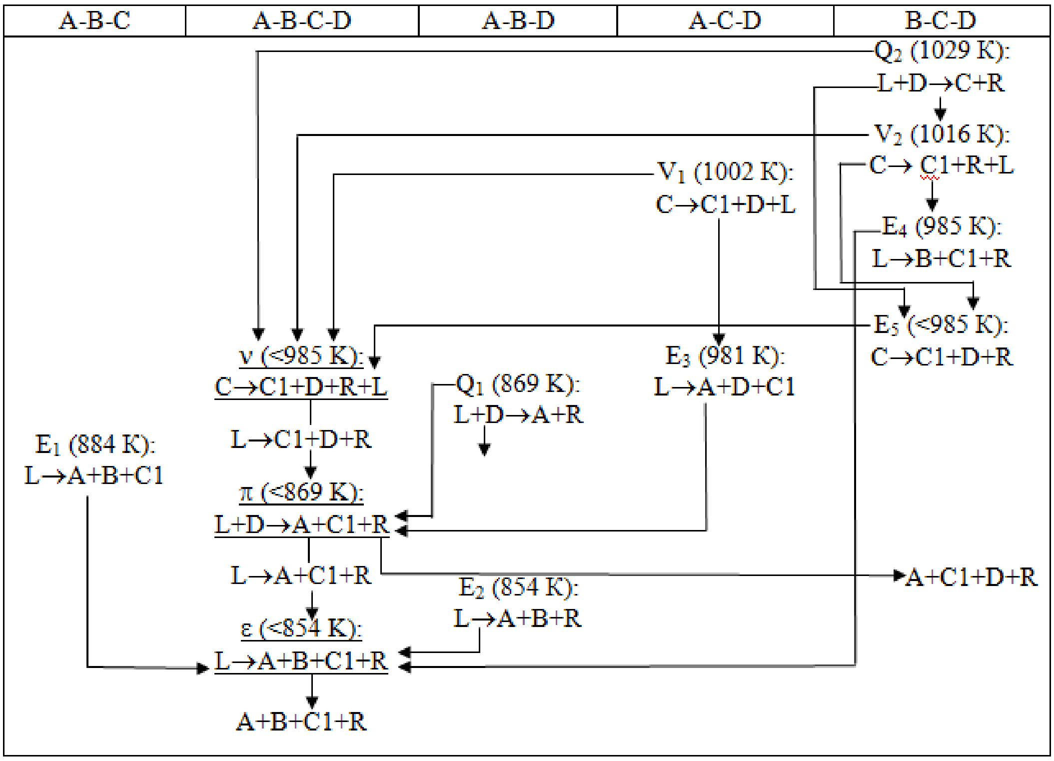

From the scheme (Table 4) it follows those three invariant reactions can be expected:

- CaF$_2$ → CaF$_2$' + LaF$_3$ + NaLaF$_4$ + L (or ν: C → C1 + D + R + L) – polymorphic transition between two modifications of calcium fluoride (C and C1) in the presence of liquid L, LaF$_3$ (D) and NaLaF$_4$ (R) compound at temperatures below 985 K;
- L + LaF$_3$ → LiF + CaF$_2$' + NaLaF$_4$ (π: L + D → A + C1 + R) – quasi-peritectic reaction at a temperature below 869 K;
- L → LiF + NaF + CaF$_2$' + NaLaF$_4$ (ϵ: L → A + B + C1 + R) – eutectic reaction at a temperature below 854 K.

In this case, the T-x-y-z diagram includes:

- 6 hypersurfaces of liquidus (Fig. 5) and 6 – of solidus ones;
- 11 pairs of solvus hypersurfaces (total – 22);
- 2 hypersurfaces of the transus;
- 22 triads of ruled hypersurfaces with a generated line (66 in total);
- 52 ruled hypersurfaces with a generated plane;
- 3 complexes, corresponding to the invariant transformations ν, π, ϵ, each of which consists of five horizontal (isothermal) hyperplanes.

All these 169 hypersurfaces serve as the boundaries of 62 phase regions:

- 6 single-phase regions I (A, B, C, C1, D, R) and 6 two-phase regions L + I;

– 12 two-phase regions I + J without liquid (A + B, A + C1, A + D, A + R, B + C1, B + R, C + D, C + R, C + C1, C1 + D, C1 + R, D + R) and 12 three-phase regions with liquid L + I + J;
– 10 three-phase regions I + J + K without liquid (A + B + C1, A + B + R, A + C1 + D, A + C1 + R, A + D + R, B + C1 + R, C + C1 + D, C + C1 + R, C + D + R, C1 + D + R) and 10 four-phase regions with liquid L + I + J + K;
– 3 four-phase regions without liquid A + B + C1 + R, A + C1 + D + R, C + C1 + D + R, and 3 five-phase regions degenerated into planar hyperplanes L + A + B + C1 + R, L + A + C1 + D + R, L + C + C1 + D + R.

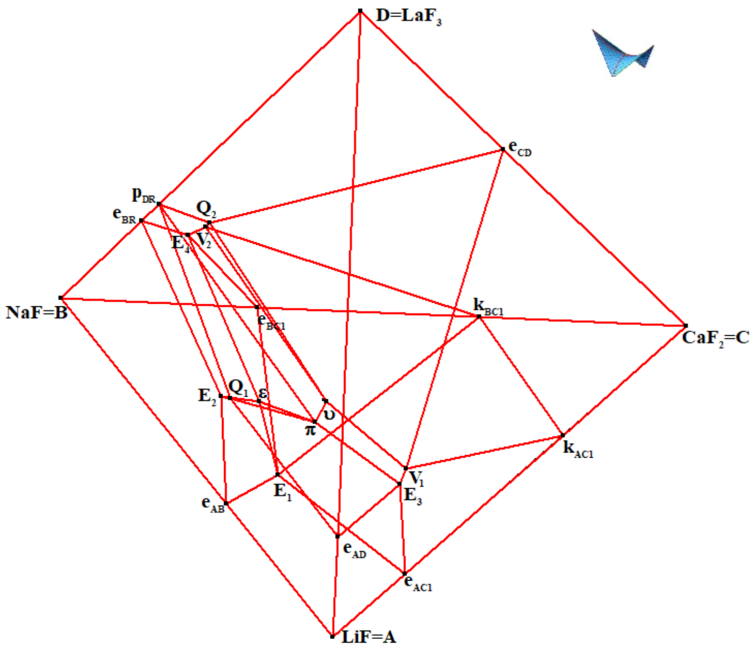

FIG. 5. Liquidus prototype 4D model: x-y-z projection of the LiF–NaF–CaF_2–LaF_3 (A-B-C-D) T-x-y-z diagram

Of course, the final confirmation (or clarification) of the prediction may be given by the experiment only.

To construct the spatial computer models of phase diagrams, it is convenient to use a special reference database for the main topological types of T-x-y and T-x-y-z diagrams. It includes the results of the phase diagrams analysis and classification for the three- and four-component systems of the main topological types [28]. This electronic guide contains 3D computer models of T-x-y diagrams: with uni- and invariant transformations, given by one, two or three binary eutectics and peritectics; with binary and ternary compounds, melting congruently or incongruently, with endothermic and exothermic phases; with the allotropy of one, two or three components, manifested in different temperature intervals; with uni- and invariant monotectic and syntectic transformations, when initial melt is decomposed into two liquids within the primary crystallization regions; with 1–3 binary monotectics or in the absence of the liquid immiscibility in binary systems; and 4D models of T-x-y-z diagrams for the six types of systems, with eutectic (peritectic) solubility gap in 1–6 border binary systems, as well as the diagrams with a binary compound, melting congruently or incongruently.

Each spatial computer model is a prototype of a phase diagram, which is able to become a perfect model of a real system after the experimental or calculated parameters (concentrations and temperatures of binary and ternary points, curvature characteristics of surfaces, according to isothermal sections and isopleths) input.

4. Conclusion

1) 3D computer models of T-x-y diagrams forming the LiF–NaF–CaF_2–LaF_3 T-x-y-z diagram have been constructed. The quality of models was confirmed by comparing of the model sections with experimental ones [23]. The ability of models to describe the history of crystallization of any melt of an arbitrary concentration or any melt belonging to a given isopleth at a given temperature, to draw crystallization paths and to simulate DTA spectra was demonstrated.

2) The T-x-y-z diagram, based on the T-x-y diagrams 3D models, has been predicted and the 4D model of its prototype has been constructed. It includes three invariant transformations: the polymorphic transition between two modifications of calcium fluoride in the passive presence of liquid, LaF$_3$ and the NaLaF$_4$ compound, the quasi-peritectic and eutectic reactions. In general, the T-x-y-z diagram may consist of 169 hypersurfaces and 66 phase regions.

3) When designing spatial computer models of phase diagrams of ternary, quaternary, and more complex systems, more attention should be paid to updating the data on their edges, including information about the initial components and compounds. In the 4D model of the LiF–NaF–CaF$_2$–LaF$_3$ diagram, considered in this paper and forming it 3D models of ternary systems, it is necessary in the future to take into account the decomposition of the binary compound NaLaF$_4$ in the sub-solidus at 330 °C [15], which is not mentioned in [23], where a binary system has been limited from below by the temperature of 600 K.

This 4D model is based on data from [23] with CaF$_2$ allotropy. However, this property of calcium fluoride is not taken into account in [29–31]. It is possible that the authors of these papers were not interested, for practical reasons, in such high temperatures (1420 K) and they did not take into account the high-temperature modification of calcium fluoride, which is stable at atmospheric pressure [32].

Nanostructured compounds (similar to Cu$_2$ZnSnSe$_4$, Ag$_2$ZnSnSe$_4$, Cu$_2$ZnSn$_{1-x}$In$_x$Se$_4$ [33–36]) should be characterized within the quaternary, quinary and more complex systems. However, research and development of multicomponent materials were carried out mainly by experiments, which is quite time-consuming and needs considerable effort. In addition to the CALPHAD technique, the new ideas to develop an integrated calculation, synthesis and characterization approach, aiming to accelerate the research efficiency, are offered [37]. Multidimensional computer model of phase diagram became an important tool to investigate the multicomponent systems. It permits to receive an adequate evaluation for the thermodynamic calculation and for the interpretation of experimental data. Computer design of materials gives a possibility to detect such nuances of micro- and nanostructure formation as 3-phase transformation type change and competition of crystals with different dispersity [38, 39].

Acknowledgements

This work was been performed under the program of fundamental research SB RAS (project 0336-2019-0008) and it was partially supported by the RFBR projects 19-38-90035, 20-21-00056.

References

[1] Beneš O., Konings R.J.M. Molten Salt Reactor Fuel and Coolant. *Comprehensive Nuclear Materials*, 2012, **3**,P. 359–389.
[2] Lutsyk V.I., Vorob'eva V.P., Zelenaya A.E. 3D Computer Model of the Ni–Cu–NiS–Cu$_2$S Subsystem T-x-y Diagram above 575 °C. *Russ. J. Phys. Chem.*, 2019, **93** (13), P. 2593–2599.
[3] Lutsyk V.I., Vorob'eva V.P. 3D Computer Models of the T-x-y Diagrams, Forming the Fe–Ni–Co–FeS–NiS–CoS Subsystem. *Russ. J. Phys. Chem.*, 2017, **91** (13), P. 2593–2599.
[4] Lukiyanchuk G., Fedorov P.P. The BaF$_2$–SnF$_4$ System. *Russ. J. Inorgan. Chem.*, 1996, **41** (5), P. 826–827.
[5] Fedorov P.P., Buchinskaya I.I., et al. Phase Diagrams of the NaF–RF$_3$ (R = Tb, Dy, Er) Systems. *Russ. J. Inorgan. Chem.*, 1996, **41** (10), P. 1715–1719.
[6] Fedorov P.P., Buchinskaya I.I., et al. Phase Diagrams of the NaF–RF$_3$ (R = Tm, Yb, Lu) Systems. *Russ. J. Inorgan. Chem.*, 1996, **41** (11), P. 1920–1924.
[7] Ratnikova I.D., Korenev Y.M., et al. Phase Diagrams of the Systems BaF$_2$–RF$_4$ (R=Zr, Hf). *Russ. J. Inorgan. Chem.*, 1997, **42** (2), P. 302–307.
[8] Stasyuk V.A., Buchinskaya I.I., et al. Phase Diagram of the CaF$_2$–SrF$_2$–NdF$_3$ System. *Russ. J. Inorgan. Chem.*, 1998, **43** (5), P. 844–848.
[9] Buchinskaya I.I., Fedorov P.P. Interaction of Lead Fluoride with Strontium and Calcium Fluorides. *Russ. J. Inorgan. Chem.*, 1998, **43** (7), P. 1106–1110.
[10] Fedorov P.P., Ivanovskaya N.A., et al. Phase Equilibria in the SrF$_2$–BaF$_2$–LaF$_3$ System. *Doklady Physical Chemistry*, 1999, **366** (4–6), P. 168–170.
[11] Zakalyukin R.M., Glazunova T.Yu., et al. Phase Equilibria in the Pb$_3$Al$_2$F$_{12}$–Ba$_3$In$_2$F$_{12}$ Section of the PbF$_2$–BaF$_2$–AlF$_3$–InF$_3$ Quaternary System. *Russ. J. Inorgan. Chem.*, 1999, **44** (10), P. 1645–1648.
[12] Fedorov P.P. Systems of Alcali and Rare-Earth Metal Fluorides. *Russ. J. Inorgan. Chem.*, 1999, **4** (11), P. 1703–1727.
[13] Korenev Yu.M., Antipov P.I., et al. Phase Diagrams for the RF$_3$–HfF$_4$ Systems (R is a rare-earth elements). *Russ. J. Inorgan. Chem.*, 2000, **45** (2), P. 164–169.
[14] Filatova N.G., Fedorov P.P. RbF–PrF$_3$ System. *Russ. J. Inorgan. Chem.*, 2000, **45** (5), P. 785–788.
[15] Fedorov P.P., Buchinskaya I.I., et al. Phase Diagrams of the NaF–RF$_3$ (R = La, Ce, Pr, Nd, Sm) Systems. *Russ. J. Inorgan. Chem.*, 2000, **45** (6), P. 949–952.
[16] Fedorov P.P., Buchinskaya I.I., et al. CaF$_2$–BaF$_2$ Phase Diagram. *Doklady Physical Chemistry*, 2005, **401** (2), P. 53–55.
[17] Fedorov P.P., Rappo A.V. NaF–CaF$_2$–YbF$_3$ Phase Diagram. *Russ. J. Inorgan. Chem.*, 2008, **53** (7), P. 1126–1129.
[18] Fedorov P.P., Buchinskaya I.I., et al. Saddle Points on the Liquidus Surfaces of Solid Solutions in the PbF$_2$–CdF$_2$–RF$_3$ Systems. *Russ. J. Inorgan. Chem.*, 1996, **41** (3), P. 445–449.
[19] Stasjuk V.A., Buchinskaya I.I., et al. Liquidus and Solidus of Fluorite Solid Solutions in the CaF$_2$–SrF$_2$–LaF$_3$ System. *Russ. J. Inorgan. Chem.*, 1998, **43** (8), P. 1266–1269.
[20] Fedorov P.P., Sobolev B.P. Conditions for the Formation of Maxima on the Fusion Curves of Solid Solutions in Salt Systems. *Russ. J. Inorgan. Chem.*, 1979, **24** (4), P. 574–575.

[21] Fedorov P.P. Geometric Thermodynamic Description of the Congruent-Melting Points of Solid Solutions in Binary and Ternary Systems. *Russian J. Inorgan. Chem.*, 2007, **52** (1), P. 116–120.

[22] Fedorov P.P. Thermodynamic-Topological Analysis of Melt Solidification in the Vicinity of Singular Points in Phase Diagrams. *Russ. J. Inorgan. Chem.*, 2005, **50** (12), P. 1933–1941.

[23] Beilmann M., Beneš O., Konings R.J.M., Fanghnel Th. Thermodynamic Investigation of the ($LiF+NaF+CaF_2+LaF_3$) System. *J. Chem. Thermodynamics*, 2011, **43**, P. 1515–1524.

[24] Lutsyk V.I., Vorobeva V.P., Computer Models of Eutectic Type T-x-y Diagrams with Allotropy. Two Inner Liquidus Fields of Two Low-Temperature Modifications of the Same Component. *J. Therm. Anal. Calorim.*, 2010, **101** (1), P. 25–31.

[25] Lutsyk V.I., Vorobeva V.P. 3D Model of the T-x-y Diagram of the Bi–In–Sn System for Designing Microstructure of Alloys. *Rus. J. Inorgan. Chem.*, 2016, **61** (2), P. 188–207.

[26] Lutsyk V.I., Zelenaya A.E., Nasrulin E.R., Bimbaev E.S. System $NaCl–CaCl_2–MgCl_2$ system: elaboration of spatial computer model of T--diagram. *Journal Melts*, 2016, **3**, P. 206–215. (In Russian)

[27] Miura S. Geometrical Approach to Reaction Schemes of Multicomponent Phase Diagrams. *J. Phase Equilibria and Diffusion*, 2006, **27** (1), P. 34–46.

[28] Lutsyk V.I., Vorob'eva V.P., Zelenaya A.E., Reference Book on the Oxide Systems Space Diagrams as a Tool for Data Mining. *Solid State Phenomena*, 2015, **230**, P. 51–54.

[29] Sobolev B.P., Fedorov P.P. Phase Diagrams of the CaF_2–(Y, Ln)F_3 Systems. I. Experimental. *J. Less-Common Metals*, 1978, **60**, P. 33–46.

[30] Švantner M., Mariani E., et al. Solid Solution with Fluorite Structure in the CaF_2–LaF_3 System. *Crystal Research and Technology*, 1979, **14** (3), P. 365–369.

[31] Fedorov P.P., Mayakova M.N., et al. Phase Diagram of the NaF–CaF_2 System and the Electrical Conductivity of a CaF_2-Based Solid Solution. *Rus. J. Inorg. Chem.*, 2016, **61** (11), P. 1472–1478.

[32] Cazorla C., Errandonea D. Superionicity and Polymorphism in Calcium Fluoride at High Pressure. *Physical Review Letters*, 2014, **113**, 235902.

[33] Sharma YC. Synthesis and characterisation of CZTSe bulk materials for thermoelectric applications. *Nanosystems: Physics, Chemistry, Mathematics*, 2020, **11** (2), P. 195–204.

[34] Dong Y., Wang H., Nolas G.S. Synthesis and thermoelectric properties of Cu excess $Cu_2ZnSnSe_4$. *Phys. Status Solidi RRL*, 2014, **8**, P. 61–64.

[35] Raju C., Falmbigl M., et al. Thermoelectric properties of chalcogenide based $Cu_{2+x}ZnSn_{1x}Se_4$. *AIP Advanced.*, 2013, **3**, 032106.

[36] Shi X.Y., Huang F.Q., Liu M.L., Chen L.D. Thermoelectric properties of tetrahedrally bonded wide-gap stannite compounds $Cu_2ZnSn_{1-x}In_xSe_4$. *Appl. Phys. Lett.*, 2009, **94**, 122103.

[37] Chang K., Meng F., et al. Theory-guided bottom-up design of the FeCrAl alloys as accident tolerant fuel cladding materials. *Journal of Nuclear Materials*, 2019, **516**, P. 63–72.

[38] Lutsyk V.I. T-x-y diagrams of lead-free soldering systems with thermodynamic contours of minimal surfaces. *Nanomaterials: Applications and Properties*, 2011, **2** (1), P. 11–19.

[39] Lutsyk V.I., Vorobeva V.P., Zelenaya A.E. 3D Computer Models of the Ag–Sb–Sn and $MgO–Al_2O_3–SiO_2$ T-x-y Diagrams. *Acta Physica Polonica*, 2018, **133** (4), P. 763–766.